Characterisation of topographical, biomechanical and maturation properties of corneocytes with respect to anatomical location

Évora, Ana S.; Zhang, Zhibing; Johnson, Simon A.; Adams, Michael J.

DOI:
10.1111/srt.13507

Document Version
Publisher's PDF, also known as Version of record

Citation for published version (Harvard):
Évora, AS, Zhang, Z, Johnson, SA & Adams, MJ 2023, 'Characterisation of topographical, biomechanical and maturation properties of corneocytes with respect to anatomical location', *Skin Research and Technology*, vol. 29, no. 11, e13507. https://doi.org/10.1111/srt.13507

Received: 20 September 2023 | Accepted: 12 October 2023

DOI: 10.1111/srt.13507

ORIGINAL ARTICLE

WILEY

Characterisation of topographical, biomechanical and maturation properties of corneocytes with respect to anatomical location

Ana S. Évora | Zhibing Zhang | Simon A. Johnson | Michael J. Adams

School of Chemical Engineering, University of Birmingham, Birmingham, UK

Correspondence
Ana S. Évora, School of Chemical Engineering, University of Birmingham, Birmingham B15 2TT, UK.
Email: A.S.M.M.Evora@bham.ac.uk

Funding information
Horizon 2020 Framework Programme

Abstract

Background: The Stratum Corneum (SC) is the first barrier of the skin. The properties of individual cells are crucial in understanding how the SC at different anatomical regions maintains a healthy mechanical barrier. The aim of the current study is to present a comprehensive description of the maturation and mechanical properties of superficial corneocytes at different anatomical sites in the nominal dry state.

Materials and methods: Corneocytes were collected from five anatomical sites: forearm, cheek, neck, sacrum and medial heel of 10 healthy young participants. The surface topography was analysed using Atomic Force Microscopy (AFM) and Scanning Electron Microscopy (SEM). The level of positive-involucrin cornified envelopes (CEs) and desmoglein-1 (Dsg1) were used as indirect measures of immature CEs and corneodesmosomes, respectively. In addition, AFM nanoindentation and stress-relaxation experiments were performed to characterise the mechanical properties.

Results: Volar forearm, neck and sacrum corneocytes presented similar topographies (ridges and valleys) and levels of Dsg1 (13–37%). In contrast, cheek cells exhibited circular nano-objects, while medial heel cells were characterized by villi-like structures. Additionally, medial heel samples also showed the greatest level of immature CEs (32–56%, $p < 0.001$) and Dsg1 (59–78%, $p < 0.001$). A large degree of inter-subject variability was found for the Young's moduli of the cells (0.19–2.03 GPa), which was correlated with the level of immature CEs at the cheek, neck and sacrum ($p < 0.05$).

Conclusion: It is concluded that a comprehensive study of the mechanical and maturation properties of corneocytes may be used to understand the barrier functions of the SC at different anatomical sites.

KEYWORDS
atomic force microscopy, corneocytes, corneodesmosomes, cornified envelopes, mechanical properties

1 | INTRODUCTION

Human skin is the interface between an organism and the external environment, hence the stratum corneum (SC), apart from posing a barrier against environmental factors,[1] and microorganisms and chemicals,[2] is also responsible for the barrier function of the skin,[3] that is, to control tissue water loss, and to accommodate mechanical loading.[4] Therefore, the SC must be flexible and able to adapt mechanically to water gradients, body movements and external pressure and shear forces. This layer is primarily composed of corneocytes, which are dead but active cells subject to a maturation process as they move through the SC to the skin surface.[5] This includes the loss of central corneodesmosomes (CDs), which culminates in a honeycomb pattern of intercellular junctions,[6,7] and the maturation of the cornified envelopes (CE) by the cross-linking of proteins and the covalent attachment of lipids.[8]

It has been suggested that the mechanical strength of the SC, particularly related to water gradients, must arise from the CEs,[9–11] on the basis that isolated keratin films swell considerably in water, almost to the point of dissolution, such that it does not display detectable elasticity.[12] The properties of CEs have been studied using different techniques: (i) immuno- and Nile red staining, (ii) mechanical resilience testing against ultrasonic waves[8] and (iii) micromanipulation evaluation of maximum compression forces.[11] The level of CE maturation has been observed to be greater in the forearm than in the face[13] and smaller in locations of fresh scars.[14] More recently, Guneri et al. showed an increase in maturation in the deeper SC of photoprotected regions of the face, compared to photoexposed ones.[8]

Furthermore, changes in the distribution of CDs have been linked to certain skin conditions, with the presence of circular nano-objects and central CDs being observed in atopic dermatitis.[15–17] These junctions are thought to, not only be involved in the barrier function of the SC,[7] but also in the mechanical resilience.[18] In fact, the high peripheral adherence of corneocytes is considered to allow them to form tight layers that are able to resist high stresses, while being impermeable to the outside medium.[18]

The previous attempts at characterizing corneocytes from different anatomical sites and skin conditions have been focused on specific cell properties, and a comprehensive understanding of the relationship between maturation (topography, CEs and CDs) and mechanical properties is still lacking. The aim of the current study was to determine the characteristics of superficial corneocytes in healthy young skin at different anatomical sites. Cells were collected from non-glabrous (forearm, cheek, neck and sacrum) and glabrous (medial heel) skin and surface properties were investigated, viz., topography, CD distribution and CE maturation, and also the mechanical properties.

2 | MATERIALS AND METHODS

2.1 | Corneocyte collection

This research project received approval from the University of Birmingham Ethics Committee (ERN-19-1398A). The study recruited a cohort of 10 able-bodied participants (six males and four females). Written, signed and dated consent was received from each participant prior to sample collection. Participants were screened to exclude those presenting active skin diseases or allergies. The ages of the participants ranged from 24 to 29 (29.6 ± 1.6) years. The mean height and weight were 1.72 ± 0.06 m and 73.1 ± 12.3 kg, respectively, with corresponding mean BMI of 24.4 ± 3.5 kg/m^2. Corneocytes were collected from the five anatomical locations via tape stripping (Sellotape, UK): forearm, cheek, neck, sacrum and medial heel, by pressing the tape gently onto the skin with gloved hands and gently removing by peeling the tape. The first tape strip was discarded to avoid the presence of contaminants, such as clothing fibres. Each tape strip was cut in four sections and used for the assessment of corneocyte topography via SEM and AFM, analysis of maturation properties (CE maturation and indirect visualization of CDs) and mechanical analysis by AFM.

2.2 | Scanning electron microscopy (SEM)

The surface topographies of corneocytes were evaluated with SEM micrographs using a table-top Hitachi TM3030 electron microscope equipped with an integrated four-segment backscattered electron detector. The samples were prepared by coating with 5 nm of gold using a Quorum Q150R ES gold sputter, utilising argon as the inert gas, with a pressure of 0.5 bar.

2.3 | CE maturity assay: CE extraction and immunostaining for involucrin and Nile red staining for lipids

Cornified envelopes were isolated from the tape using a previously described methodology.[19] Briefly, half of one tape section was extracted with 750 mL of dissociation buffer containing 100 mM Tris-HCl pH 8.0, 5 mM EDTA (ethylenediaminetetraacetic acid), 2% SDS (sodium dodecyl sulphate) and 20 mM DL-dithiothreitol (Sigma Aldrich Dorset, UK). Tape sections were extracted in the dissociation buffer for 10 min at 75°C and centrifuged at room temperature for 10 min at 5000 g. The extracted CEs were washed (three times) in washing buffer: 20 mM Tris-HCl pH 9.0, 5 mM EDTA, 0.2% SDS and 10 mM DL-dithiothreitol and suspended in 1 × PBS buffer (Sigma Aldrich Dorset, UK). Extracted CEs were transferred on to a Polysine-coated microscope slide (5 μL, VWR international Ltd, Leicestershire, UK) and incubated overnight in a humidified chamber at 4°C with a primary monoclonal antibody against involucrin (1:100, mouse anti-human involucrin SY5, ABCAM, Cambridge, UK). The antibody solution was washed with PBS three times for 5 min before adding the secondary antibody Alexa-Fluor 488-labeled goat anti-mouse IgG antibody (1:200, ABCAM, Cambridge, UK) for 60 min at room temperature (in the dark). The slides were washed with 1 × PBS (three times for 5 min) and mounted with 20 μg/mL Nile red (Sigma Aldrich, Dorset, UK) in 75% glycerol solution (w/w).

2.4 | Immunostaining for Dsg1

The immunostaining protocol for desmoglein-1 (Dsg1) was performed as previously described.[19] Briefly, corneocytes attached to a tape section were washed with 1 × PBS (10 min) and incubated with a P23 mouse monoclonal antibody against the extracellular domain of Dsg1 (Progen, Heidelberg, Germany) at 4°C overnight. This was followed by incubation with Alexa-Fluor 488-labeled goat anti-mouse IgG antibody (1:200, ABCAM, Cambridge, UK), for 60 min at room temperature (20°C) in the dark. The samples were mounted with anti-fade fluorescence mounting medium (ABCAM, Cambridge, UK).

2.5 | Image analysis

Five non-overlapping fluorescence images were acquired in total for each CE and each Dsg1 sample with a field of view of 720 × 580 μm. It involved a 10× objective magnification and an analysis using a Leica DMRBE microscope (Leica Microsystems, USA) equipped with PL-Fluotar 5 × /0.12 and 10 × /0.30 lenses mounted with a Cool-LED pE-300 series blue-illumination source at the wavelength of 460 nm and with a Motic Pro 252 microscope camera. Image analysis was done as previously described.[19] Briefly, CE maturation was evaluated using a sequential approach: after application of a Gaussian filter, images were converted to either an 8-bit map (for total cell number count) or divided in RGB channels (to count cells staining for Alexa-Fluor 488, that is, positive to involucrin—green channel). The Huang threshold followed by Watershed command was applied to define CE borders and the cells with a surface area of 300–2000 μm^2 were counted based on average values reported in literature.[5] For the distribution of Dsg1, the ratio of pixels expressing Dsg1 to the total area in pixels was counted in two random regions of interest (ROIs) of 5000 μm^2 that contained corneocytes, as previously established and described.[17] Initially, images were transformed in 8-bit maps and a Huang threshold was applied. This was followed by the Watershed command and using "Analyse Particle" command to count number of pixels.

2.6 | Atomic force microscopy

Atomic force microscopy (AFM) imaging and nanoindentation experiments were performed under environmentally controlled conditions (35% RH and 25°C) using an AFM operated in Tapping Mode (TM) and Force Spectroscopy, respectively (Nanowizard 4, Bruker, JPK BioAFM Berlin, Germany). Standard imaging tips, with a nominal spring constant of 40 N/m and resonance frequency of 300 kHz, were used (NCHV-A, Bruker AFM Probes, Inc). Corneocytes were extracted by pressing the tape section onto a microscope glass slide by overnight incubation in xylene. Cells attached to the glass slide were first imaged to study their surface topography (512 × 512 pixels, 40 × 40 μm), and a zoom-in TM image was then obtained in the centre of each cell (5 × 5 μm, 512 × 512 pixels) and used as a region of interest (ROI) for the nanoindentation measurements. These consisted of the analysis of 64 force curves (indentation force, F,versus indentation depth, h) extracted from 8 × 8 matrices, with points spaced 625 nm apart. The geometry of AFM tips was obtained as described in the Supplementary Information (S1). Briefly, an elastomer (polydimethylsiloxane, PDMS) was used as a reference material for nanoindentation; the value of the Young's modulus of the PDMS was measured by micromanipulation. AFM loading curves were analysed using a combination of a sixth-order polynomial smoothing function and power law equations to obtain a tip-radius function, that is, contact radius, a, as a function of contact depth, h_c. Nanoindentation measurements on corneocytes involved loading-pause-unloading cycles, with a maximum applied force of 1.5–2 μN. Stress-relaxation was studied over a 4 s pause period, after the maximum force setpoint at loading was reached. The pause segment was set at constant height and the force relaxation was measured.

2.7 | AFM data analysis

2.7.1 | Elastic deformation

The Young's modulus, E, of corneocytes was calculated from the unloading portion of the force curves using the Oliver-Pharr method:[20]

$$E = \frac{\sqrt{\pi}}{2}\left(1-\nu^2\right)\frac{S_0}{\sqrt{A}} \tag{1}$$

where S_0 is the unloading stiffness at the maximum force, F_{max}, which corresponds to the maximum indentation depth, h_{max}, and $A = \pi a^2$ is the contact area, where a is the contact radius.[21] The Poisson's ratio for corneocytes, ν, was assumed to be 0.4, based on the value for keratin.[22]

Corneocytes are elastoplastic materials,[9] so that the contact depth is related to h_{max} by the expression:[20]

$$h_c = h_{max} - h_s \tag{2}$$

where h_s is the surface elastic deflection at the perimeter of the contact, which is given by the following expression:[20]

$$h_s = \phi\frac{F_{max}}{S_0} \tag{3}$$

The unloading stiffness, $S_0 = dF/dh$ at $h = h_{max}$ was obtained by differentiating the following polynomial fit to the upper 80% the unloading curve with respect to h, and determining the slope at h_{max}:[23]

$$F = C_e h^2 - \left(2C_e h_f\right)h + C_e h_f^2 \tag{4}$$

where C_e and h_f are fitting parameters. The geometric factor, ϕ, was assumed to be 0.73 for a conical indenter, following the work of Oliver and Pharr.[24]

The tip contact radius functions, $a(h_c)$, for all three tips employed in this study are shown in Figure S1. These functions are required to

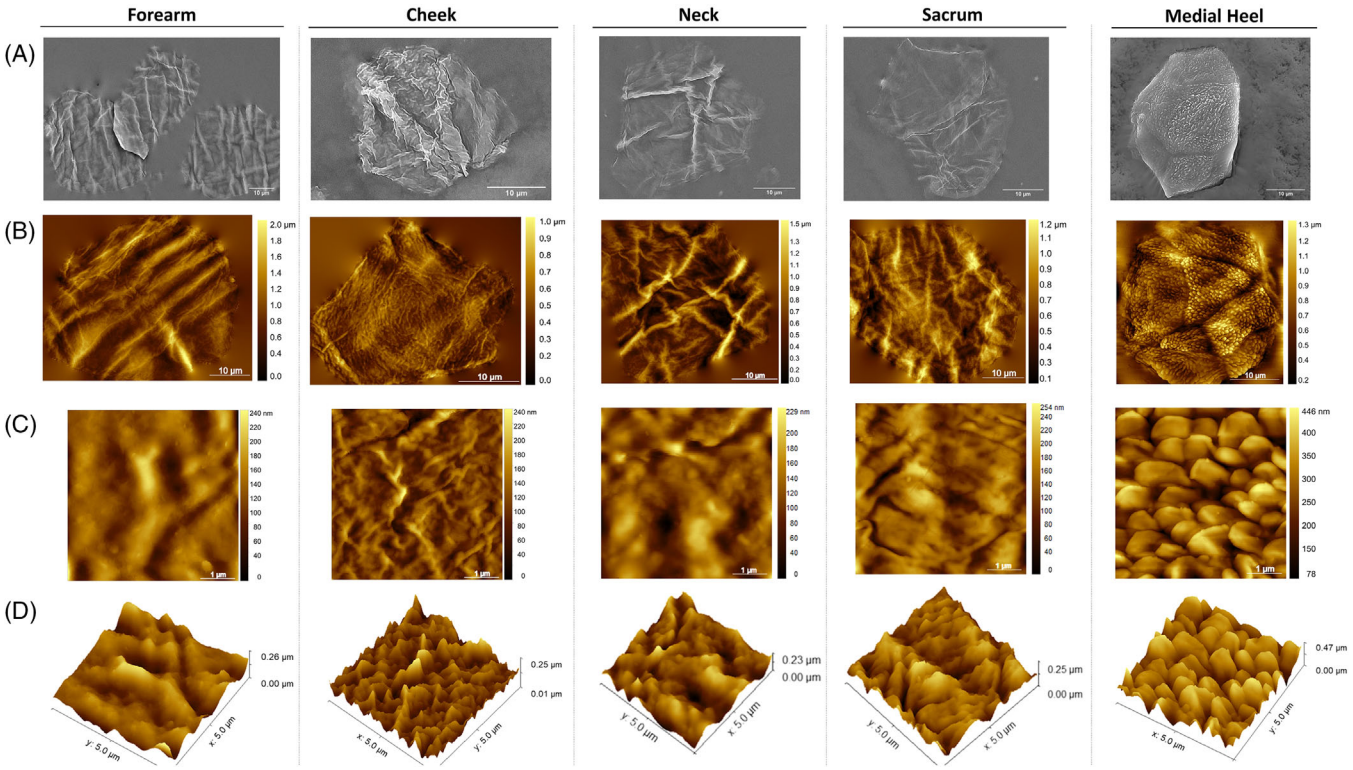

FIGURE 1 (A) SEM and (B) AFM analysis revealed differences in the topography of corneocytes from superficial skin. Forearm, neck and sacrum presented ridges and valleys across the cell surface, while cheek usually exhibited CNOs; and medial heel cells were characterized by villi-like structures. Colour bar corresponds to height (μm) in AFM topography. Scale bars = 10 μm. (C) Individual corneocytes were analysed at high magnification (5 × 5 μm) using tapping mode AFM. Scale bars = 1 μm. (D) 3D representation of the aforementioned zoomed regions.

TABLE 1 Roughness values measured from Zoom-in TM AFM images of the corneocytes.

	Roughness (nm)		Cell area (μm^2)	
Anatomical region	S_q	S_a	AFM	CE size
Forearm	54.5 ± 13.0	42.8 ± 10.5	1148.3 ± 230.8	780.5 ± 102.3
Cheek	82.8 ± 17.8	65.6 ± 14.2	695.3 ± 97.4	554.2 ± 81.0
Neck	46.6 ± 12.4	37.5 ± 9.9	956.0 ± 87.7	694.4 ± 173.5
Sacrum	31.2 ± 12.8	24.6 ± 9.8	1079.0 ± 194.6	772.2 ± 227.1
Medial heel	102.2 ± 28.4	82.5 ± 23.3	811.5 ± 125.1	579.8 ± 174.6

Sq (root mean square height) and Sa (arithmetical mean height) for an area of 25 μm^2 are given for a cohort of 10 participants (five cells per participant and anatomical site). The projected cell area was measured directly from AFM topographical images and from extracted CEs. Results are presented as mean ± 1 SD.

calculate the contact area for each indent at h_{max} in Equation (1) from the contact depth, h_c, obtained using Equations (2) and (3).

2.7.2 | Stress-relaxation analysis

The rate-dependent properties of the corneocytes were calculated by fitting a Prony series to the stress-relaxation curves:

$$F(t) = B_0 + B_1 e^{-t/\tau_1} + B_2 e^{-t/\tau_2} \quad (5)$$

from which the coefficients B_0, B_1 and B_2 were obtained, as well as the characteristic relaxation times, τ_1 and τ_2. Assuming the decay in the force arises from viscoplastic dissipation, the force can be related to the time-dependent hardness $H(t) = F(t)/A$:

$$F(t) = \pi a^2 H(t) \quad (6)$$

and thus,

$$H(t) = C_0 + \sum_{i=1}^{2} C_i e^{-t/\tau_i} \quad (7)$$

So that the coefficients C_0, C_1 and C_2 can be calculated by:

$$C_i = \frac{B_i}{\pi a^2} \tag{8}$$

where $i = (0, 1, 2)$. Finally, the instantaneous hardness, H_0 and the long-term hardness, H_∞, can, then, be estimated using the following equations:

$$H_0 = \sum_{i=0}^{2} C_i \tag{9}$$

and

$$H_\infty = C_0 \tag{10}$$

2.8 | Statistical analysis

Raw data were imported into IBM SPSS Statistics (version 27) for analysis and assessed for normality using probability plots and the Shapiro-Wilk test for each site and participant. While the topographical data revealed normal distributions, the maturation properties (%INV+ and %Dsg1) and AFM nanoindentation data showed a non-normal distribution. Accordingly, ANOVA followed by Bonferroni test or Kruskal-Wallis test were employed to investigate whether the anatomical sites had differences in maturation and mechanical properties, respectively. The Mann-Whitney test was used to investigate differences between genders. Tests were considered statistically significant at a 5% level ($p < 0.05$). The Spearman's correlational analysis was employed to investigate the relationships between the mechanical and maturation properties.

3 | RESULTS

3.1 | Topography of corneocytes at different anatomical locations

Representative topographical images of superficial corneocytes from five anatomical locations: forearm, cheek, neck, sacrum and medial heel, of young adult skin obtained using SEM and AFM tapping mode are shown in Figures 1A and 1B. They displayed hexagonal or pentagonal shapes and anatomical site-dependent topographical features. Volar forearm, neck, and sacrum corneocytes showed similar features in the form of ridges across the surface, organized in peaks and valleys. In contrast, most cheek cells showed "circular nano-objects" (CNOs) at the surface, as first described by Riethmüller.[15] Moreover, corneocytes from the plantar region of the foot had a surface divided in "isles" of "villi-like" structures. At a greater magnification, villous protrusions in medial heel cells are prominent (Figures 1C and 1D). They were related to an increase in surface roughness (Table 1) as expressed by the root mean square height (S_q) of 102.2 ± 28.4 nm and were significantly different ($p < 0.001$) from the forearm, neck, and sacrum, which had values of S_q of about 54, 46 and 31 nm, respectively. The corrugated surface of cheek cells, generally populated by CNOs, also showed significantly greater roughness (82.8 ± 17.8 nm) values than the forearm ($p < 0.05$), neck ($p < 0.01$) and sacrum ($p < 0.001$).

The average size of the corneocytes via AFM topography was generally greater than those obtained by fluorescence microscopy of extracted CEs (Table 1). This may be due to the multi-step process used to extract CEs from the tape and separate them individually. Although the level of structural changes provoked by the extraction protocol was not studied, some structural changes to the keratin matrix are expected due to the denaturing nature of some materials (e.g., SDS), which may render a less rigid form. Nonetheless, both methods resulted in similar size trends, that is, cheek cells were generally smaller than forearm (AFM: $p < 0.01$; CEs: $p < 0.001$), neck (CEs: $p < 0.01$) and sacrum cells (CEs: $p < 0.001$). Moreover, medial heel cells were statistically smaller than those from the forearm ($p < 0.05$) and sacrum (CEs: $p < 0.001$).

3.2 | CE maturity levels at different anatomical sites

The maturity level of the CEs was evaluated from the percentage of immature CEs, which was defined as the ratio between involucrin-positive CEs to the total number of CEs. Representative fluorescence microscopy images are shown in Figure 2A for participants 2 and 7, exemplifying low and high levels of CE maturity, respectively. Individual data are presented in Figure 3A. All anatomical sites, apart from the medial heel, which had a coefficient of variation (CV) of 17%, showed considerable inter-subject variability, with the forearm and neck exhibiting the highest (CV 68 and 71%, respectively), followed by the cheek and sacrum (CVs 49%, 48%, respectively). In fact, participants 1–3 and 10 exhibited relatively greater amounts of INV+ CEs at all body sites, while participants 4–9 showed smaller levels of immature CE. The cohort data are presented in Table 2. The mean values of immature CEs were similar at the forearm (16.7%), neck (18.4%) and sacrum (20.4%) and relatively greater, but not statistically significant, at the cheek (24.4%). Medial heel had the greatest level of CE immaturity (47.8%, $p < 0.001$).

3.3 | Distribution of Dsg1 at different anatomical sites

The distribution of the CDs was indirectly analysed by immunostaining of Dsg1, which is an intercellular adhesion protein mainly expressed in the upper layers of the skin (Figure 2B).[7] Relatively smaller inter-subject variability was found for %Dsg1 (Figure 3B), being the greatest at the forearm and cheek (CV 31 and 28%, respectively), followed by the neck (CV 19%), and the sacrum (CV 15%) and being the smallest at the medial heel (CV 9%). A honeycomb pattern of Dsg1 was prevalent in the forearm, neck and sacrum samples, while cheek samples usually displayed a dispersed signal (Figure 2B). This was distinct from medial heel samples, in which Dsg1 was ubiquitously found over the

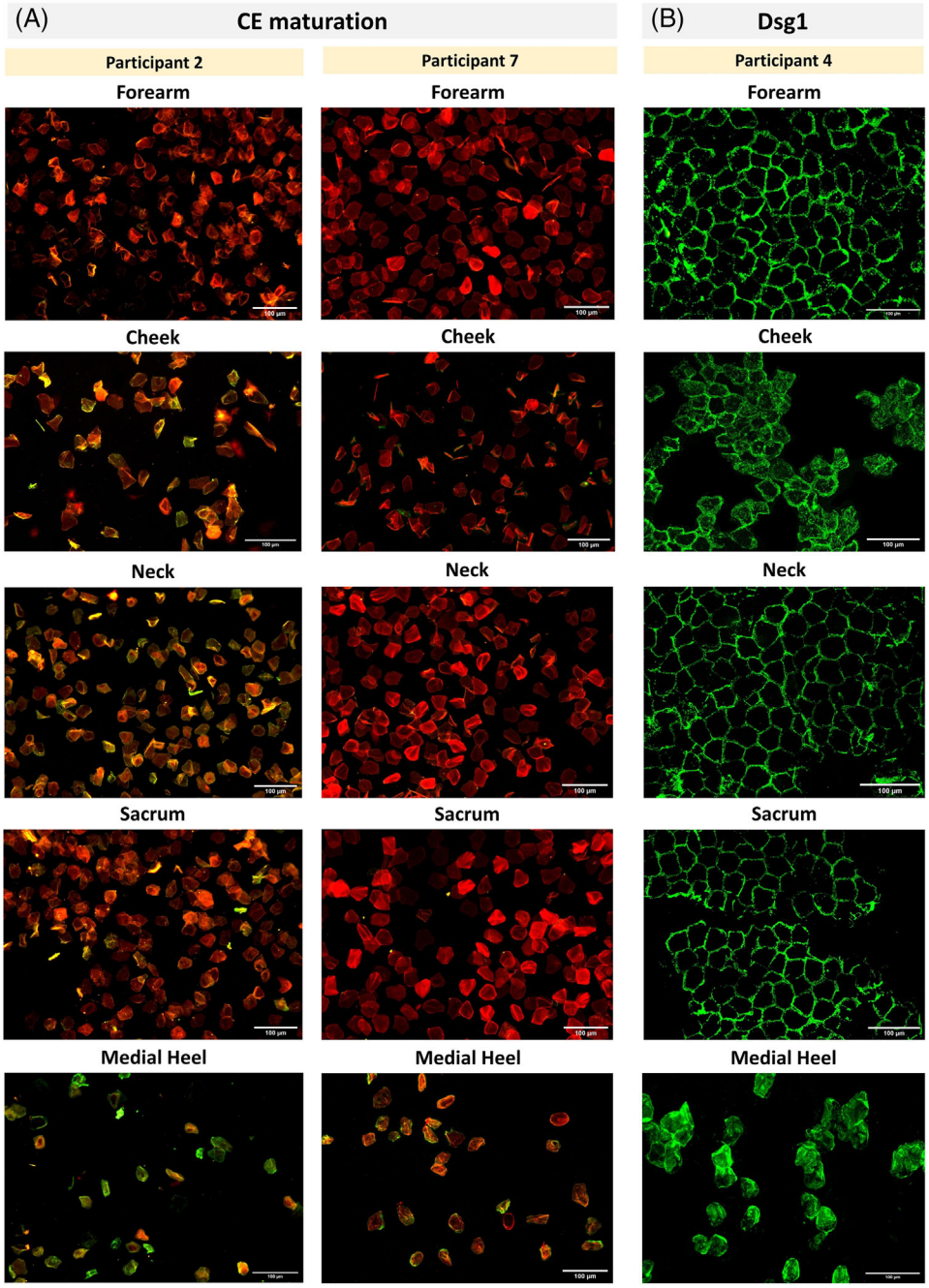

FIGURE 2 (A) Images of forearm, cheek, neck, sacrum and medial heel superficial CEs using double staining: immunostaining against INV (green) and Nile red (red) against lipids to quantify the degree of CE maturation. Participants 2 and 7 (P2 and P7) are presented as representative of low and high CE maturity. Forearm, neck and sacrum corneocytes of P7 stained strongly with Nile red, while the cheek exhibited less lipids at the surface. Medial heel cells stained strongly in green for INV. P2 had higher levels of involucrin-positive CEs at all body sites. (B) Distribution of Dsg1 at the surface of superficial corneocytes as an indirect measure of CDs for participant 4. Forearm, neck, and sacrum cells have a typical honeycomb structure with Dsg1 mostly presented at the cell periphery. Cheek corneocytes showed a Dsg1 distribution dispersed on the surface, but not with a ubiquitous manner as shown in medial heel cells. Scale bar = 100 μm.

cell surface. In fact, the mean value found for medial heel samples was 67.2%, being the greatest of the anatomical sites studied ($p < 0.001$), which was followed by the cheek (46.1%, $p < 0.01$) (Table 2). Volar forearm, neck and sacrum samples showed similar amounts of Dsg1, with mean values of 23.0%, 21.3% and 18.1%, respectively. Interestingly, while tape strip samples of forearm, neck and sacrum were characterized by uniform layers of cells, cheek samples revealed patches of corneocytes, while the medial heel samples usually showed individual cells or groups of three or four cells, but never in a regular layer.

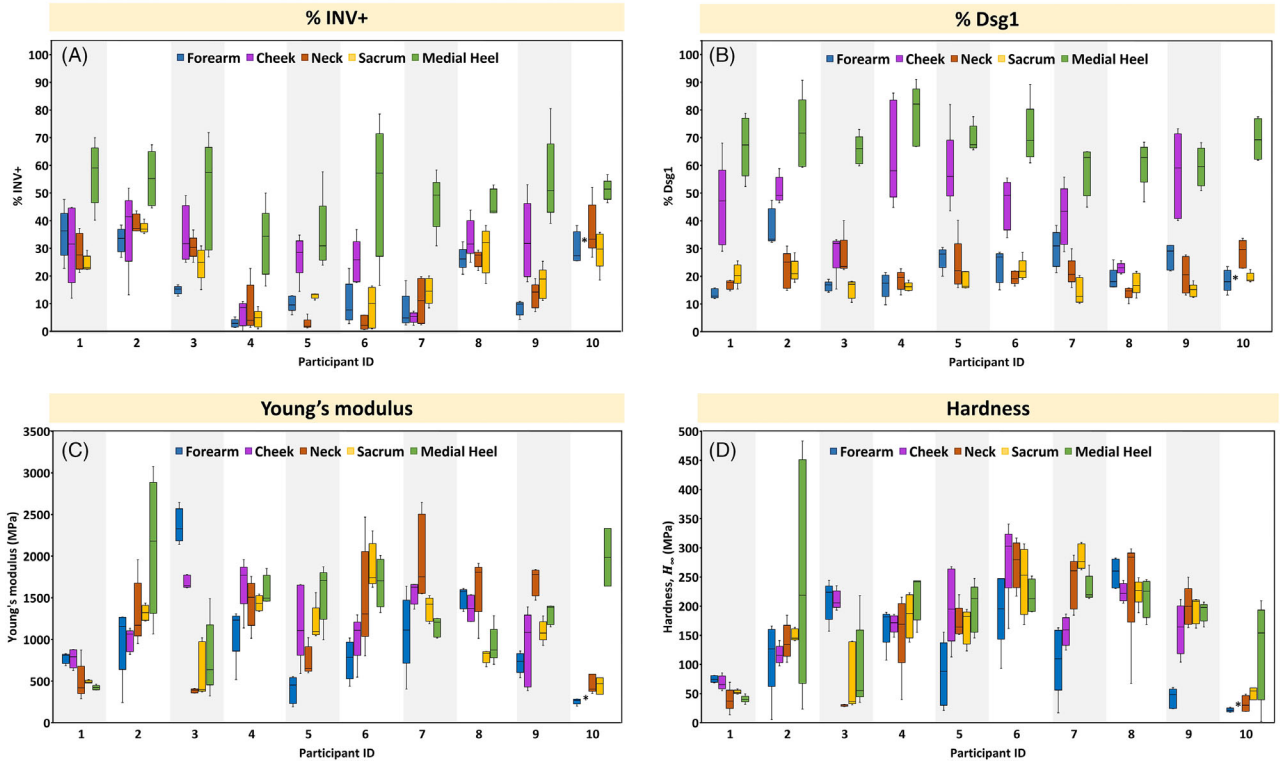

FIGURE 3 Box-and-whisker plots of individual data of (A) % INV CEs, (B) % Dsg1, (C) elastic modulus and (D) hardness ($\mathbf{H}_\infty$) for 10 subjects. The upper and lower whiskers represent the highest and lowest datum within 1.0 IQR (interquartile range). * indicates missing data—participant sample was not collected.

3.4 | Biomechanical properties of corneocytes

The biomechanical properties of corneocytes are presented in Table 2. Individual moduli data revealed considerable inter-subject variability (Figure 3C). In fact, participants 1, 3 and 10 displayed the smallest Young's moduli, with medians of ~ 770, 1231, 465, 490 and 780 MPa for forearm, cheek, neck, sacrum and medial heel, respectively. While the remainder of the cohort presented medians of ~ 994, 1210, 1500, 1320 and 1560 MPa for forearm, cheek, neck, sacrum and medial heel, respectively. Interestingly, the median for the forearm modulus was the smallest (890 MPa, $p = 0.077$), while the greatest was found for the medial heel (1.43 GPa). The rate-dependent properties are shown in Table 2. Individual data for H_0 (Figure 3D) and H_∞ revealed inter-subject variability similar to that observed for the Young's moduli. Statistical differences were not found between anatomical sites, although the median values tended to be smaller for the forearm and greater for the medial heel.

3.5 | Correlational analysis between corneocyte biomechanics and CE maturation level

Based on the substantial inter-subject variability found for the corneocyte properties, a correlational analysis was employed to determine if they could be interrelated (Table 2). As expected, values of the Young's modulus were correlated to H_0 and H_∞, that is, greater cell stiffness correlated with greater hardness values as related to the yield strain, H_0/E. There were no correlations between these properties and the relaxation times. Furthermore, the cell stiffness was correlated with the level of immature CEs at the cheek, neck and sacrum, that is, participants having softer cells, also presented a higher level of immature CEs ($p < 0.05$). The hardness values correlated to CE maturity only at the neck and sacrum ($p < 0.05$).

3.6 | Influence of gender on corneocyte properties

To understand the origin of the inter-subject variability found in the maturation and biomechanical properties of corneocytes, intrinsic factors were considered. However, since the cohort was relatively homogeneous in age and BMI, the only apparent intrinsic factor was gender: four female and six male participants. Consequently, the data were pooled according to gender and tested for differences amongst the two groups, using Mann-Whitney test for pairwise comparisons. The results are shown in Figure 4. Female participants generally had lower levels of immature CEs and Dsg1 (Figures 4A and 4B) and smaller cells (Figure 4D). These differences were mainly found at the forearm, neck and sacrum ($p < 0.05$). Superficial cheek corneocytes did not show differences between the female and male participants. Although median values of the Young's modulus were generally smaller

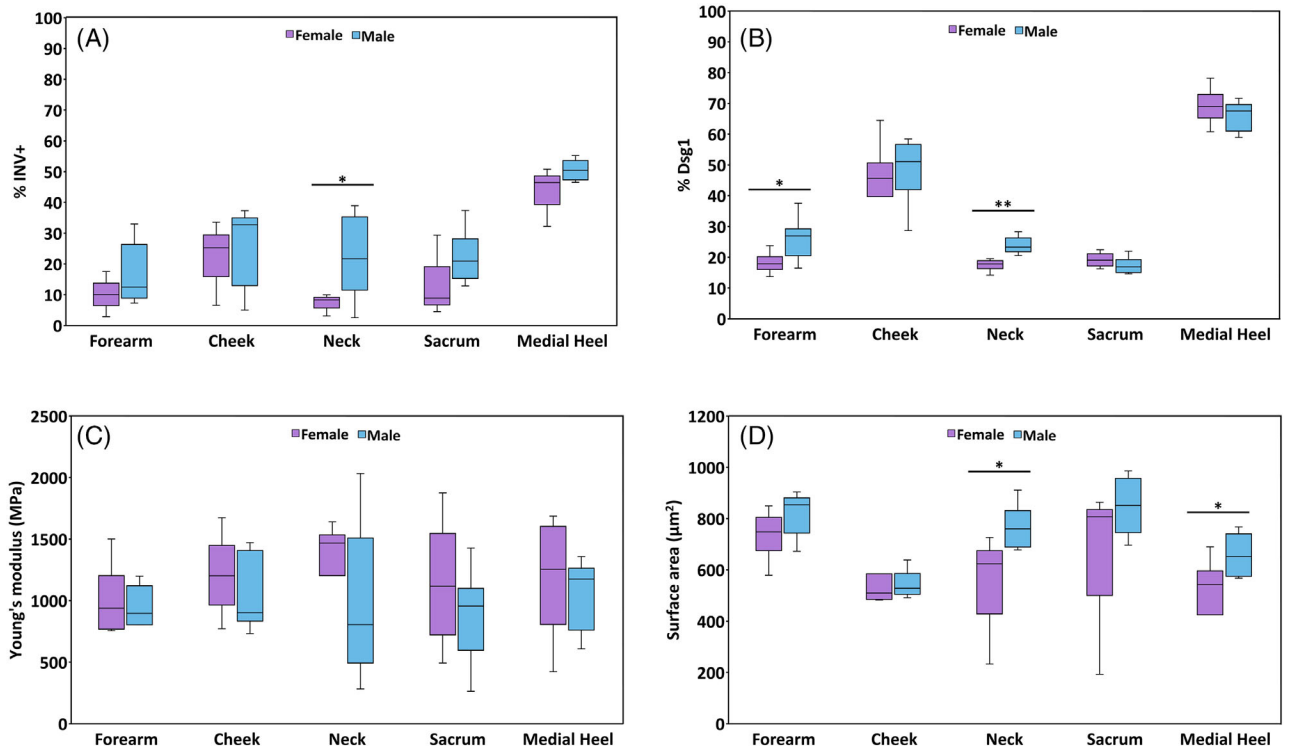

FIGURE 4 Differences between the properties of corneocytes according to gender. Box-whisker plots for the level of immature CEs (A), % Dsg1 (B), Young's modulus (C) and cell size (D) per body site and gender. The upper and lower whiskers represent the highest and lowest datum within 1.0 IWR (interquartile range). $^{*}p < 0.05$, $^{**}p < 0.01$ by the Mann-Whitney test performed for each male-female pair per body site.

for male participants, there were no statistically significant differences registered.

4 | DISCUSSION

Although the different properties of corneocytes have been studied using a range of techniques,[6–9,11] there has not been a comprehensive examination relating maturation and the biomechanical properties. The aim of the current study was to characterize the superficial corneocytes collected from five anatomical sites from non-glabrous and glabrous skin. The topographical and maturation properties were similar for volar forearm, neck, and sacrum cells. They had a relatively smooth surface ($S_a \sim 25–42$ nm) characterized by ridges and valleys. Moreover, they displayed immature CEs levels ranging from ~3–40% and levels of Dsg1 in the range 13–37% (Figure 3A and 3B). In contrast, cheek and medial heel cells had distinct topographical features with increased surface roughness of ~ 65 and 82 nm in terms of the values of S_a, respectively, with cheek corneocytes presenting CNOs, and samples from the medial heel revealing prominent villi-like structures (Figures 2C and 2D). Both sites also showed the highest levels of Dsg1, with mean values of 46 and 67, respectively (Table 2). Moreover, medial heel cells also had the highest levels (around 48%) of immature CEs of the five anatomical sites studied (Table 2).

The differences in maturation and topography between the cheek and neck corneocytes demonstrate that anatomically close body sites can have different SC characteristics. Guneri et al. previously showed that corneocytes from different facial sites (photoprotected and photoexposed regions) exhibit different maturation levels, with a greater amount of INV+ CEs being present in the cheek (40%) compared to the post-auricular site (15%).[8] In the present study, although not statistically significant, the level of immature CEs tended to be greater at the cheek (24%), compared to the neck (18%). Moreover, the two sites were topographically distinct and showed different levels of Dsg1. In fact, neck corneocytes were smoother ($S_a = 37.5 \pm 9.9$ nm, Table 1) and characterized by a honeycomb pattern of Dsg1 (Figure 2). While cheek cells had a rougher surface ($S_a = 65.6 \pm 14.2$ nm, $p < 0.01$) and a dispersed pattern of Dsg1 (Figure 2). Cheek corneocytes may be challenged by a variety of external factors, the most relevant being UV radiation. Engebretsen et al.[25] observed significant differences in the Dermal Texture Index (CNOs) for the cheek and hand cells between summer and winter. In addition, Lipsky et al. observed differences in the pattern and distribution of Dsg1 with increasing doses of UVB irradiation,[26] and Biniek et al. proposed that UV radiation influences the intercellular lipids and CD distribution.[27] Nevertheless, neck corneocytes exhibit characteristics of a mature SC (Figures 1 and 2). In fact, lower levels of transepidermal water loss and greater water contents were previously found at the neck compared to the cheek,[28] indicating that the former is characterized by a healthy barrier function, which is consistent with the characteristics observed in this study.

To fully characterize the biomechanical properties, nanoindentation and stress-relaxation experiments were performed using AFM.

TABLE 2 Maturation and biomechanical properties of corneocytes characterized by elastoviscoplastic behaviour and expressed as % INV+, % Dsg1, Young's modulus, **E**, relaxation times, tau, and hardness, $\mathbf{H_0}$ and $\mathbf{H_\infty}$.

Anatomical region	Mean ± 1 SD		Median (min-max)					Parameter		Correlation coefficient
	% INV+	% Dsg1	*E* (MPa)	τ_1 (s)	τ_2 (s)	H_0 (MPa)	H_∞ (MPa)			
Forearm	16.7 ± 11.4	23.0 ± 7.0	889.6 (258.2-2361.6)	0.12 (0.10-0.16)	1.90 (1.55-2.64)	152.6 (34.2-302.6)	111.0 (21.8-256.8)	*E*	H_∞	0.678*
									H_0	0.818**
Cheek	24.4 ± 12.0	46.2 ± 12.8**	1206.5 (772.2-1690.1)	0.12 (0.10-0.14)	1.78 (1.57-2.80)	224.6 (82.0-329.0)	169.9 (68.6-289.1)	*E*	% INV	−0.791*
Neck	18.4 ± 13.1	21.3 ± 4.1	1379.6 (385.2-1972.9)	0.12 (0.11-0.13)	1.97 (1.57-2.79)	220.8 (36.9-321.1)	164.6 (29.8-262.9)	*E*	% INV	−0.695*
									H_∞	0.887*
									H_0	0.891**
								H_0	% INV	−0.810*
								H_∞	% INV	−0.781*
Sacrum	20.4 ± 9.9	18.1 ± 2.8	1145.9 (450.7-1876.0)	0.12 (0.11-0.12)	1.75 (1.53-2.19)	232.4 (61.9-333.0)	174.9 (51.3-284.0)	*E*	% INV	−0.882**
									H_∞	0.777*
									H_0	0.770**
								H_0	% INV	−0.666 ($p = 0.05$)
Medial heel	47.8 ± 8.0***	67.2 ± 5.8***	1433.6 (422.6-2126.9)	0.12 (0.11-0.13)	2.05 (1.65-2.62)	251.8 (48.5-282.3)	206.9 (40.6-251.2)	*E*	H_∞	0.602 ($p = 0.07$)
									H_0	0.599 ($p = 0.07$)

Given the non-normal distribution of the AFM data, values are presented as median and range of values (min-max) ($n = 5$ cells per body site and participant and collected from 10 subjects).
*$p < 0.05$. **$p < 0.01$, ***$p < 0.001$ by ANOVA followed by Bonferroni test for maturation properties or Kruskal-Wallis test for cell mechanics. The summary of significant Spearman correlations between corneocyte maturation and mechanical properties are also presented.

Interestingly, there were no significant differences in the stiffness and hardness between the anatomical regions studied. However, there was a large inter-subject variability for the stiffness, hardness, and CE maturity level. When employing a correlational analysis between the Young's modulus and %INV+ CEs, a negative correlation was found at the cheek, neck and sacrum (Table 2), suggesting that participants with lower levels of immature CEs, usually have stiffer cells (Table 2). Guneri et al. challenged the ability of the maturity assay used in the current study to provide biomechanical information about the CE.[8] The authors showed that otherwise considered immature CEs (high level of INV+ CEs) are mechanically mature when their rigidity is evaluated using an ultrasonic wave test. Indeed, the double staining technique used here treats the hydrophobicity of the CE as the indicator of CE maturity. Although most authors relate this to CE rigidity, there is not any evidence that this is the case. Cornified lipid envelope formation might not necessarily occur with stiffening of the CE, which depends on the cross-linking of its proteins. However, the analysis of inter-subject variability in this study suggests that there is a relationship between the maturity level of the CE based on its hydrophobicity and the biomechanical properties at least at three of the five anatomical sites evaluated.

Previously, the stiffness of the SC in full-thickness samples of glabrous skin was shown to be greater than non-glabrous skin measured in AFM experiments.[29] However, in the present study, although the stiffness of cells tended to be greater at the medial heel, there was not a statistical significance in the results, which may arise from the small number of cells analysed per participant. This is surprising considering the load-bearing function of the plantar regions of the skin. In fact, it has been suggested that plantar SC is mechanically adapted to sustain high pressures and keratin 9, only expressed in suprabasal layers of glabrous skin, has been thought to provide such strength.[8,30] The current study was subject to a relatively small number of participants and, particularly, of cells (five cells per anatomical site and participant), which may contribute to the lack of statistical significance in the results. This is one of the most important limitations of using AFM since the measurements are extremely time consuming and require a great number of force curves for making valid conclusions.

Samples collected from the male participants were generally more immature than those from the females (Figure 4), presenting higher levels of immatures CEs at the neck and sacrum ($p < 0.05$) and greater proportions of Dsg1 at the forearm and neck ($p < 0.001$). Previous studies found correlations between the CE surface area and their maturity, that is, usually larger cells were associated with greater levels of mature CEs.[31,32] However, in the current study, although displaying higher levels of immature CEs, the cells from male participants were also the largest (Figure 4) at the forearm, sacrum, medial heel ($p < 0.001$) and neck ($p < 0.05$). A similar trend in cell size for the forearm has been previously observed between pre-menopausal women and men.[33] Cells at the neck and sacrum were generally softer for the male participants, although not statistically significant.

The current study was limited to a relatively small cohort of 10 participants from white (Caucasian) ethnicity. In addition, only 4 out of 10 participants were female and there was only a small variation in the age or BMI. Consequently, the results obtained by combining data according to gender must be taken with caution since a larger cohort would be necessary to corroborate any conclusions.

The current results may assist in understanding the role of the SC in sustaining pressure and shear. Differences were not found between cells from non-glabrous skin, except for the cheek, which had increased levels of Dsg1. In contrast, there is an indication that load bearing body sites (heel) benefit from stronger cohesion between SC cells, suggested by a uniform distribution of CDs. Interestingly, although glabrous and non-glabrous skin present different surface maturation properties, they are similar in terms of the mechanical properties.

In summary, the current study evaluated the surface and biomechanical properties of superficial corneocytes in the nominally dry state from five anatomical sites: forearm, cheek, neck, sacrum and medial heel, which were collected from 10 healthy young participants. Cells at the forearm, neck and sacrum showed similar surface topography and levels of Dsg1, different from cheek ($p < 0.01$) and medial heel ($p < 0.001$) corneocytes. The later were characterized by high levels of Dsg1 and distinct topographical features, with cheek cells generally presenting circular nano-objects at the cell surface, and medial heel cells being characterized by villi-like structures. Although there was considerable inter-subject variability, there were no differences in the mechanical properties across anatomical sites either related to cell stiffness ($E = 0.25–2.36$ GPa) or initial and equilibrium hardness ($H_0 = 34–333$ MPa and $H_\infty = 22–290$ MPa). However, there was a correlation between the proportion of immature CEs and the stiffness of the corneocytes, that is, stiffer corneocytes were usually associated with a greater proportion of CE maturity. Additionally, the male participants showed a greater proportion of CE immaturity and Dsg1 and larger CEs.

ACKNOWLEDGEMENTS

This work was supported by the European Union's Horizon 2020 research and innovation programme under the Marie Skłodowska-Curie grant agreement No. 811965 (Project STINTS Skin Tissue Integrity under Shear).

CONFLICT OF INTEREST STATEMENT

The authors have no conflicts of interest.

DATA AVAILABILITY STATEMENT

The data that support the findings of this study are available from the corresponding author upon request.

ETHICS STATEMENT

This study was approved by the Health Research Authority committee (ERN-19-1398A) and written informed consent was obtained from patients prior to commencing the study.

ORCID

Ana S. Évora https://orcid.org/0000-0003-1562-6105
Zhibing Zhang https://orcid.org/0000-0003-2797-9098
Simon A. Johnson https://orcid.org/0000-0001-6621-7622
Michael J. Adams https://orcid.org/0000-0001-9648-7308

REFERENCES

1. Matsui T, Amagai M. Dissecting the formation, structure and barrier function of the stratum corneum. *Int Immunol*. 2015;27(6):269-280.
2. Dayan N, Wertz PW. *Innate Immune System of Skin and Oral Mucosa: Properties and Impact in Pharmaceutics, Cosmetics, and Personal Care Products*. John Wiley & Sons; 2011.
3. Kalia YN, Alberti I, Sekkat N, Curdy C, et al. Normalization of stratum corneum barrier function and transepidermal water loss in vivo. *Pharm Res*. 2000;17(9):1148-1150.
4. Leyva-Mendivil MF, Page A, Bressloff NW, Limbert G. A mechanistic insight into the mechanical role of the stratum corneum during stretching and compression of the skin. *J Mech Behav Biomed Mater*. 2015;49:197-219.
5. Évora AS, Adams MJ, Johnson SA, Zhang Z. Corneocytes: relationship between structural and biomechanical properties. *Skin Pharmacol Physiol*. 2021;34(3):146-161.
6. Goto H, Tada A, Ibe A, Kitajima Y. Basket-weave structure in the stratum corneum is an important factor for maintaining the physiological properties of human skin as studied using reconstructed human epidermis and tape stripping of human cheek skin. *Br J Dermatol*. 2020;182(2):364-372.
7. Naoe Y, Hata T, Tanigawa K, Kimura H, Masunaga T. Bidimensional analysis of desmoglein 1 distribution on the outermost corneocytes provides the structural and functional information of the stratum corneum. *J Dermatol Sci*. 2010;57(3):192-198.
8. Guneri D, Voegeli R, Gurgul SJ, Munday MR, Lane ME, Rawlings AV. A new approach to assess the effect of photodamage on corneocyte envelope maturity using combined hydrophobicity and mechanical fragility assays. *Int J Cosmet Sci*. 2018;40:207-216.
9. Beard JD, Guy RH, Gordeev SN. Mechanical tomography of human corneocytes with a nanoneedle. *J Invest Dermatol*. 2013;133(6):1565-1571.
10. Milani P, Chlasta J, Abdayem R, Kezic S, Haftek M. Changes in nano-mechanical properties of human epidermal cornified cells depending on their proximity to the skin surface. *J Mol Recognit*. 2018;31(9):e2722.
11. Harding CR, Long S, Richardson J, et al. The cornified cell envelope: an important marker of stratum corneum maturation in healthy and dry skin. *Int J Cosmet Sci*. 2003;25(4):157-167.
12. Park A, Baddiel C. Rheology of stratum corneum II: A physico-chemical investigation of factors influencing the water content of the corneum. *J Soc Cosmet Chem*. 1972;23:13-21.
13. Hirao T, Denda M, Takahashi M. Identification of immature cornified envelopes in the barrier-impaired epidermis by characterization of their hydrophobicity and antigenicities of the components. *Exp Dermatol*. 2001;10(1):35-44.
14. Kunii T, Hirao T, Kikuchi K, Tagami H. Stratum corneum lipid profile and maturation pattern of corneocytes in the outermost layer of fresh scars: the presence of immature corneocytes plays a much more important role in the barrier dysfunction than do changes in intercellular lipids. *Br J Dermatol*. 2003;149(4):749-756.
15. Riethmüller C. Assessing the skin barrier via corneocyte morphometry. *Exp Dermatol*. 2018;27(8):923-930.
16. Riethmuller C, McAleer M, Koppes S, et al. Filaggrin breakdown products determine corneocyte conformation in patients with atopic dermatitis. *J Allergy Clin Immunol*. 2015;136(6):1573-1580.e2.
17. Igawa S, Kishibe M, Honma M, et al. Aberrant distribution patterns of corneodesmosomal components of tape-stripped corneocytes in atopic dermatitis and related skin conditions (ichthyosis vulgaris, Netherton syndrome and peeling skin syndrome type B). *J Dermatol Sci*. 2013;72(1):54-60.
18. Guo S, Domanov Y, Donovan M, et al. Anisotropic cellular forces support mechanical integrity of the Stratum Corneum barrier. *J Mech Behav Biomed Mater*. 2019;92:11-23.
19. Évora AS, Abiakam N, Jayabal H, et al. Characterisation of superficial corneocytes in skin areas of the face exposed to prolonged usage of respirators by healthcare professionals during COVID-19 pandemic. *J Tissue Viability*. 2023;32(2):305-313.
20. Oliver WC, Pharr GM. An improved technique for determining hardness and elastic modulus using load and displacement sensing indentation experiments. *J Mater Res*. 1992;7(6):1564-1583.
21. Popov VL, Heß M, Willert E. Normal contact without adhesion. In: *Handbook of Contact Mechanics: Exact Solutions of Axisymmetric Contact Problems*. Springer; 2019:5-65.
22. Zhenxing H, Gaosheng L, Huimin X, Tao H, Pengwan C, Fenglei H. Measurement of Young's modulus and Poisson's ratio of human hair using optical techniques. *Proceedings of SPIE*. 7522; 2010: 75222Q.
23. Fischer-Cripps AC. Contact mechanics. In: Fischer-Cripps AC, ed. *Nanoindentation*. Springer; 2002:1-19.
24. Oliver WC, Pharr GM. Measurement of hardness and elastic modulus by instrumented indentation: Advances in understanding and refinements to methodology. *J Mater Res*. 2004;19(1):3-20.
25. Engebretsen K, Kezic S, Riethmüller C, et al. Changes in filaggrin degradation products and corneocyte surface texture by season. *Br J Dermatol*. 2018;178(5):1143-1150.
26. Lipsky ZW, German GK. Ultraviolet light degrades the mechanical and structural properties of human stratum corneum. *J Mech Behav Biomed Mater*. 2019;100:103391.
27. Biniek K, Kaczvinsky J, Matts P, Dauskardt RH. Understanding age-induced alterations to the biomechanical barrier function of human stratum corneum. *J Dermatol Sci*. 2015;80(2):94-101.
28. Chirikhina E, Chirikhin A, Xiao P, Dewsbury-Ennis S, Bianconi F. In vivo assessment of water content, trans-epidermial water loss and thickness in human facial skin. *Appl Sci*. 2020;10(17):6139.
29. Boyle C, Plotczyk M, Villalta S, et al. Morphology and composition play distinct and complementary roles in the tolerance of plantar skin to mechanical load. *Sci Adv*. 2019;5(10):eaay0244.
30. Fu DJ, Thomson C, Lunny DP, et al. Keratin 9 is required for the structural integrity and terminal differentiation of the palmoplantar epidermis. *J Invest Dermatol*. 2014;134(3):754-763.
31. Mohammed D, Matts P, Hadgraft J, Lane M. Variation of stratum corneum biophysical and molecular properties with anatomic site. *AAPS J*. 2012;14(4):806-812.
32. Raj N, Voegeli R, Rawlings AV, et al. A fundamental investigation into aspects of the physiology and biochemistry of the stratum corneum in subjects with sensitive skin. *Int J Cosmet Sci*. 2017;39(1):2-10.
33. Fluhr JW, Pelosi A, Lazzerini S, Dikstein S, Berardesca E. Differences in corneocyte surface area in pre- and post-menopausal women. *Skin Pharmacol Physiol*. 2001;14(suppl 1):10-16.

SUPPORTING INFORMATION

Additional supporting information can be found online in the Supporting Information section at the end of this article.

How to cite this article: Évora AS, Zhang Z, Johnson SA, Adams MJ. Characterisation of topographical, biomechanical and maturation properties of corneocytes with respect to anatomical location. *Skin Res Technol*. 2023;29:e13507. https://doi.org/10.1111/srt.13507